Sunflower Array of Infinitesimal Dipoles for Constrained Antenna Modeling

Onat, Nehir Berk ; Yarovoy, Alexander; Aslan, Yanki

DOI
10.23919/EuCAP60739.2024.10501600

Publication date
2024

Document Version
Final published version

Published in
Proceedings of the 2024 18th European Conference on Antennas and Propagation (EuCAP)

Sunflower Array of Infinitesimal Dipoles for Constrained Antenna Modeling

Nehir Berk Onat[1], Alexander Yarovoy[2], Yanki Aslan[3]
Microwave Sensing, Signals and Systems Group, Department of Microelectronics,
Faculty of Electrical Engineering, Mathematics, and Computer Science,
Delft University of Technology, Delft, The Netherlands
{[1]*N.B.Onat,* [2]*A.Yarovoy,* [3]*Y.Aslan*}*@tudelft.nl*

***Abstract*—The sunflower array topology concept is introduced, for the first time, to the constrained infinitesimal dipole modeling (IDM) technique to increase the computational efficiency and reduce the modeling errors. The concept is applied to embedded element pattern predictions via matrix inversion. A novel study on the impact of the type and orientation of the dipoles on the IDM performance in pattern mean square error (MSE) and stability against noise (linked to the matrix condition number) is conducted. A 5 by 5 patch antenna array modeled with 81 dipoles is used for demonstration. It is shown that using magnetic dipoles (oriented in the direction of a radiating edge of the patch) in IDM yields the optimal performance. Besides, the sunflower topology significantly lowers the MSE (by 5 dB, on average), while reducing the condition number by a factor of 10.**

***Index Terms*— antenna pattern prediction, fast antenna modeling, Fermat spiral, infinitesimal dipoles.**

I. Introduction

Infinitesimal dipole modeling (IDM) is a well-developed technique in formulating the fields generated by an arbitrary antenna [1]. It has been used in various applications including electromagnetic emission and interference characterization in printed circuit boards [2], [3], antenna diagnostics [4], self and mutual admittance computation in arrays [5], source identification and pattern prediction in near- and far-field [6].

In IDM, the actual antenna volume is replaced by an array of (both electric, $e-$ and magnetic, $m-$type) infinitesimal dipoles (IDs), the locations, orientations and moments (complex excitations) of which are to be determined [7]. In general, metaheuristic optimization algorithms, such as Genetic Algorthm [7], [8], Invasive Weed Optimization [5] and Differential Evolution [2], are used to find out the parameter values that minimize the difference between the fields of the actual antenna and the fields predicted by the IDM. Such techniques suffer from large computational time and complexity in the case of characterization of large antennas [9], or when dynamic modeling is needed for a large amount of training dataset [3].

Constrained IDM was introduced to improve the algorithm efficiencies. In [10], it was shown that for planar antenna geometries, dipoles distributed only on the main radiation surface provide accurate fields. In [11], dipoles with fixed positions (on a Cartesian grid) and orientations were used. In [5], only e-type dipoles were considered in IDM, while in [2], only m-type dipoles were employed. Using a single type (e or m) of dipole and single orientation (x, y, or z) reduces the degrees-of-freedom solely to the dipole moments. In that case, the excitation of each dipole can be efficiently determined by solving a set of linear equations [4], [10]. However, due to the inversion of a Vandermonde-type matrix [12] with a high condition number, the number and topology of the dipoles become critical [13]. For performance stability of IDM against noise, both the condition number and errors in the estimated fields should be kept low. Towards the aim of creating irregularity in the array topology and reducing the number of dipoles, an iterative convex optimization algorithm was implemented in [9]. However, this algorithm brings additional computational complexity and results in a customized array topology for the device under test.

In this paper, we propose, for the first time, to apply the sunflower array topology concept (studied in [14], [15] for grating lobe suppression) in constrained IDM to eliminate the use of optimizers (in minimizing the pattern error and the number of dipoles) for the best computational efficiency in a reasonable accuracy. We also present a novel discussion, driven by mathematical and physical insights, on the impact of the selected (common) type and orientation of the dipoles on the predicted patterns.

The rest of the paper is organized as follows. Section II formulates the problem by introducing a modeling example with an antenna under test and the application of IDM (with conventional square-grid and the proposed sunflower array topologies) in its co-polarized far-field pattern formulation. Section III presents and discusses the numerical results. Section IV concludes the paper.

II. Problem Formulation and Proposed Solution

A. Antenna Under Test (AUT)

For this work, a planar array with equally spaced 5 by 5 pin-fed patch antennas is designed as illustrated in Fig. 1. The center and corner elements, highlighted in yellow, are selected to demonstrate the performance of the proposed approach at the embedded pattern level. The application of the proposed IDM on the total array pattern on broadside is also studied. The design parameters of the array can be found in Table I.

B. Implementation of Constrained IDM

Although each $e-$ and $m-$dipole in the ID array contributes to achieving the desired radiated field, only $y-$ and $z-$oriented

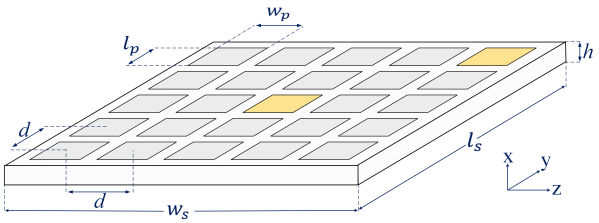

Fig. 1. 5-by-5 planar array of patch antennas as AUT. Selected elements are indicated as yellow.

TABLE I
VALUES OF ARRAY DESIGN PARAMETERS

Center frequency	2.85 GHz	**Substrate length** (l_s)	0.36 mm
Patch length (l_p)	33.71 mm	**Substrate width** (w_s)	0.36 mm
Patch width (w_p)	33.71 mm	**Substrate height** (h)	1.6 mm
Spacing (d)	0.5λ	**Permittivity** (ϵ_r)	2.2

IDs are essential in the constrained IDM [10] since the AUT is placed on $y-z$ plane as shown in Fig. 1. Table II summarizes the far-field expression of the IDs depending on the dipole type, orientation and polarization. In Table II, I_y^e, I_z^e, I_y^m and I_z^m, are the dipole currents, θ and ϕ are the spherical angles, η is the free space impedance. For the n-th ID, $C_n(\theta,\phi)$ is formulated as:

$$C_n(\theta,\phi) = \mathrm{j}wl_0\frac{\mu}{4\pi r}\mathrm{e}^{-\mathrm{j}kr}\mathrm{e}^{\mathrm{j}k(\sin\theta\sin\phi y_n+\cos\theta z_n)} \quad (1)$$

which is a common multiplication factor for different orientation and polarization of the ID with a length of l_0 at a far distance of r from its location (y_n, z_n). The formulation in (1) can be represented in a matrix form depending on the sampling of θ and ϕ. In this work, this matrix is converted into the vectorial form by concatenating its columns to fit into the problem formulation.

Since the co-polarization component of the AUT is along the ϕ direction, the $z-$oriented $e-$dipole has no contribution. In this way, the total number of contributing components reduces from four to three. This study focuses on each dipole type and orientation to analyze the prediction performances from a mathematical perspective. From a physical perspective, as the radiation of each patch antenna element of the AUT can be approximated by two magnetic dipoles along the z-axis (on the radiating edges of the patch), working with the $z-$oriented $m-$dipoles becomes more meaningful.

TABLE II
ELECTRIC FAR-FIELDS RADIATED BY IDS

Type	Orien.	Pol.	Electric Fields
Electric	y	θ	$E^e_{\theta,y}(\theta,\phi) = -\cos\theta\sin\phi I_y^e C(\theta,\phi)$
		ϕ	$E^e_{\phi,y}(\theta,\phi) = -\cos\phi I_y^e C(\theta.\phi)$
	z	θ	$E^e_{\theta,z}(\theta,\phi) = \sin\theta I_z^e C(\theta,\phi)$
		ϕ	$E^e_{\phi,z}(\theta,\phi) = 0$
Magnetic	y	θ	$E^m_{\theta,y}(\theta,\phi) = -\frac{1}{\eta}\cos\phi I_y^m C(\theta,\phi)$
		ϕ	$E^m_{\phi,y}(\theta,\phi) = \frac{1}{\eta}\cos\theta\sin\phi I_y^m C(\theta,\phi)$
	z	θ	$E^m_{\theta,z}(\theta,\phi) = 0$
		ϕ	$E^m_{\phi,z}(\theta,\phi) = -\frac{1}{\eta}\sin\theta I_z^m C(\theta,\phi)$

In formulating the constrained IDM problem, the dipole currents are the complex coefficients to be determined in order to obtain the actual radiation pattern with low errors and high stability against noise. Towards this aim, the problem can fundamentally be described as:

$$\mathbf{Ax} = \mathbf{q} \quad (2)$$

where $\mathbf{q}$ is the electric far-field of the considered element or array (in the column vector form), $\mathbf{x}$ is a column vector comprises the set of IDs coefficients, $\mathbf{A}$ is a matrix describes the total electric field of an array of infinitesimal dipoles and can be expressed as:

$$\mathbf{A}_p^t = \mathbf{F}_p^t(\theta,\phi)\cdot\Big[\langle\mathbf{C}_1(\theta,\phi)\rangle \quad \dots \quad \langle\mathbf{C}_N(\theta,\phi)\rangle\Big] \quad (3)$$

where $\langle\mathbf{C}_n(\theta,\phi)\rangle$ represents the vectorial form of (1) obtained by concatenating its columns, $\mathbf{F}_p^t(\theta,\phi)$ is the multiplier of the $p-$oriented (i.e., $y-$ or $z-$) and $t-$type (i.e., $m-$ or $e-$) ID (see Table II), and N is total number IDs in the array. It is important to note that the polarization of the electric field in (3) is ϕ as it is the co-polarization component, and the polarization subscripts used in Table II are omitted here for brevity.

C. Proposed Solution

The proposed methodology aims to estimate the dipole coefficients, $\mathbf{x}'$, to achieve a reasonably accurate desired radiation field, $\mathbf{q}'$ that matches $\mathbf{q}$. A straightforward solution, $\mathbf{x}'$, can be found by utilizing the least squares solution:

$$\mathbf{x}' = (\mathbf{A}^{\mathrm{H}}\mathbf{A})^{-1}\mathbf{A}^{\mathrm{H}}\mathbf{q} \quad (4)$$

if $\mathbf{A}^{\mathrm{H}}\mathbf{A}$ is invertable. Although the mentioned inverse matrix exists, the resulting $\mathbf{x}'$ has high sensitivity due to the high condition number of $\mathbf{A}$, which has a form of Vandermonde-type matrix caused by the successive raise as a polynomial power by the dipole position as can be seen in (1). The matrix $\mathbf{A}$ is required to be relaxed by regularization to reduce the condition number, and to achieve a noise-tolerant solution. To achieve this, a two-step approach is proposed in this work:

1) A relatively small stochastic noise matrix $\boldsymbol{\xi}$ is introduced to the matrix $\mathbf{A}$ as in [16], [17], where $\boldsymbol{\xi} \to \mathcal{N}(\mu, \sigma^2)$ with the mean $\mu = 0$ and the variance $\sigma^2 = 10$.
2) IDs form a sunflower array topology.

It is also important to mention that only the field magnitudes are formulated by IDM in this work; nevertheless, the work can be extended into complex patterns by including the phase information. This will bring an additional performance trade-off as the stochastic noise used for matrix regularization has an impact on the phases.

III. NUMERICAL RESULTS

Due to the mutual coupling (MC) effect, the embedded element patterns (EEPs) are highly affected by the adjacent elements depending on their positions. The center and a corner

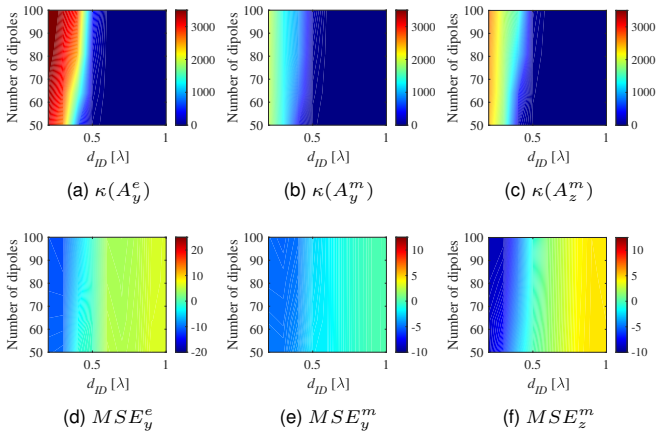

Fig. 2. Regular topology analysis for the center element of the AUT: (a)-(c) condition number of the matrix **A** for the specified dipole types and orientations, (d)-(f) MSE between the full-wave generated and predicted EEPs of the AUT's center element for the selected ID types and orientations.

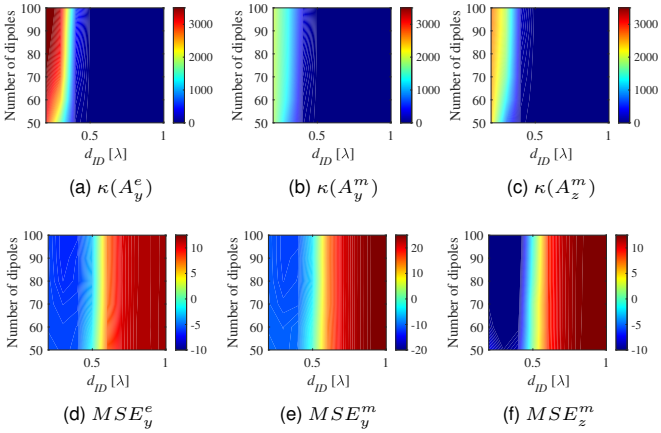

Fig. 3. Sunflower topology analysis for the center element of the AUT: (a)-(c) condition number of the matrix **A** for the specified ID types and orientations, (d)-(f) MSE between the full-wave generated and predicted EEPs of the AUT's center element for the selected ID types and orientations.

element are selected in this work to demonstrate the effectiveness of the proposed methodology under pattern variations. Furthermore, the array far-field pattern is reconstructed with the predicted EEPs by the constrained IDM and compared with the full-wave simulation. The sunflower ID array topology performance is compared with the conventional regular square topology for different ID types and orientations. This analysis is carried by jointly considering the condition number of the matrix **A**, $\kappa(\mathbf{A})$, and the mean squared error (MSE) between the simulated and IDM predicted far-field magnitudes:

$$MSE_p^t = 10\lg\left(\frac{1}{N_s^2}\sum_{i,j=1}^{N_s}\left(|E_{\text{CST}}(\theta_i,\phi_j)| - |E_p^t(\theta_i,\phi_j)|\right)^2\right) \quad (5)$$

where N_s is the number of samples for θ and ϕ, E_{CST} is the full-wave simulated electric field of the chosen element or the array in the far-field region that is generated by the commercial full-wave simulator CST.

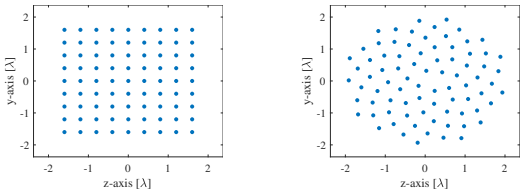

Fig. 4. 81-element conventional regular and proposed sunflower topologies for the constrained IDM.

A. Center Element

The generated EEP of the center element (EEP_{CST}) is taken as a benchmark pattern. The $\kappa(A_p^t)$ and the MSE_p^t are analyzed to find an optimum topology for the constrained IDM. First, the IDs are positioned on the conventional square-grid topology and the number of dipoles are varied with the uniform dipole element spacing (d_{ID}) for a given dipole type and orientation as shown in Fig. 2.

As the element spacing increases, the correlation in the matrix **A** decreases, and the condition number is reduced. This is common to all cases as shown in Fig. 2. When d_{ID} becomes larger, the IDs start to exceed the defined aperture size. As the aperture is not sufficiently sampled, the MSE increases.

On the other hand, having a small element spacing between the IDs decreases the error between the original and predicted patterns, however, it increases the condition number. Likewise, increase in the number of IDs causes higher condition number and better MSE when the element spacing is kept low (i.e., $d_{\text{ID}} < 0.5\lambda$), which can be seen as a slight diagonal slope in Fig. 2. Although having a high number of dipoles in the constrained IDM can provide more precise predictions, the precision is also limited by the d_{ID} and aperture size.

Moreover, different dipole orientations and types affect the MSE (due to the differences in the angular dependence given in Table II) and the condition number. In line with the physical reasoning, $z-$oriented $m-$dipole-based constrained IDM shows a better MSE result while having an acceptable $\kappa(A_z^m)$ for $d_{\text{ID}} < 0.5\lambda$ as illustrated in Fig. 2c and 2f.

As for the sunflower array, the distance from the center to the n-th element, is formed as [14]:

$$\rho_n = d_{ID}\sqrt{\frac{n}{\pi}} \quad (6)$$

with the angular displacement of the n-th element:

$$\varphi_n = 2\pi n\beta \quad (7)$$

where β is the parameter that controls the angular displacement between two adjacent elements. As β is taken as $\beta = \frac{\sqrt{5}+1}{2}$, the sunflower topology is obtained. In Eq. (6), d_{ID} refers to the mean distance between the adjacent elements. Therefore, the analysis of element spacing in the framework of this paper is the mean distance in the sunflower topology.

By introducing the sunflower topology into the constrained IDM, the MSE is significantly improved for all cases as shown in Fig. 3. Due to its unique topology with maximal degrees of

TABLE III
RESULTS OF THE EEP PREDICTION WITH 81-ELEMENT IDM FOR AUT'S CENTER ELEMENT

Dipole	MSE_{reg}	MSE_{sun}	$\kappa(\mathbf{A})_{reg}$	$\kappa(\mathbf{A})_{sun}$
$y-$orien. $e-$ID	-2.4 dB	-6 dB	2467.8	402.4
$y-$orien. $m-$ID	-4.5 dB	-5.5 dB	951.9	203.5
$z-$orien. $m-$ID	-4.7 dB	-11.5 dB	1121.2	133.29

TABLE IV
RESULTS OF THE EEP PREDICTION WITH 81-ELEMENT IDM FOR AUT'S CORNER ELEMENT

Dipole	MSE_{reg}	MSE_{sun}	$\kappa(\mathbf{A})_{reg}$	$\kappa(\mathbf{A})_{sun}$
$y-$orien. $e-$ID	-2 dB	-5.6 dB	2479.1	402.3
$y-$orien. $m-$ID	-3.3 dB	-4.31 dB	946.4	203.4
$z-$orien. $m-$ID	-4.3 dB	-8 dB	1122.9	133.3

freedom, the proposed technique captures more details of the EEP and hence provides a wide range of low MSEs, allowing more flexibility in selecting the condition number. Besides, it decreases the condition number in a similar manner compared to the square-grid topology, as illustrated in Fig. 3a, 3b and 3c. Similar to the regular topology, the $z-$oriented $m-$dipoles have the lowest error particularly when the dipole spacing is lower than 0.5λ.

To visualize the field prediction performance of the proposed topology in the IDM, 81 IDs with a dipole spacing of $d_{\text{ID}} = 0.4\lambda$ were chosen as an example case study as the both topologies are illustrated in Fig. 4. The simulation results are listed in Table III. It is observed that the proposed topology outperforms the conventional topology in the constrained IDM, and the $z-$oriented $m-$dipole gives the best results as expected. The error is kept below -11 dB while the condition number is reduced from 1121.2 to 133.29, which provides significant stability against noise and stability of the matrix A during the inversion process.

Beyond the error and condition number quantification, Fig. 5 illustrates an excellent agreement between the full-wave simulated and proposed methodology. It is also important to mention that the edges of the EEPs generated by the proposed constrained IDM show small unmatched regions depending on the dipole type and orientation, which brings different θ, ϕ dependence in the ID pattern. In fact, each ID case has a better prediction ability on different edges; the $z-$oriented $m-$dipoles provide good prediction for the angles $60 < |\phi| < 90$, while the $y-$oriented $e-$dipoles are better at $150 < \theta$ and $\theta < 30$. Although the effect of mismatches in these regions is small on the MSE (due to low field magnitudes), this is still a small drawback of the proposed contraint with a single-type dipole simplification.

B. Corner Element

The EEP of a corner element is expected to be different than the middle element due to the finite size of the ground plane and the MC effects caused by the other adjacent elements. For this purpose, a corner element, which is highlighted in Fig. 1 with yellow, was chosen as the second case study.

The same analysis for the condition number and MSE is conducted as done in Sec. III-A. The simulations show very similar results that are obtained for the middle element as provided in Fig. 2 and 3.

The simulation results for the study case with 81 IDs are illustrated in Fig. 6 and Table IV. Since the EEP of the corner element shows more asymmetrical behavior than the middle element, the field prediction becomes more challenging.

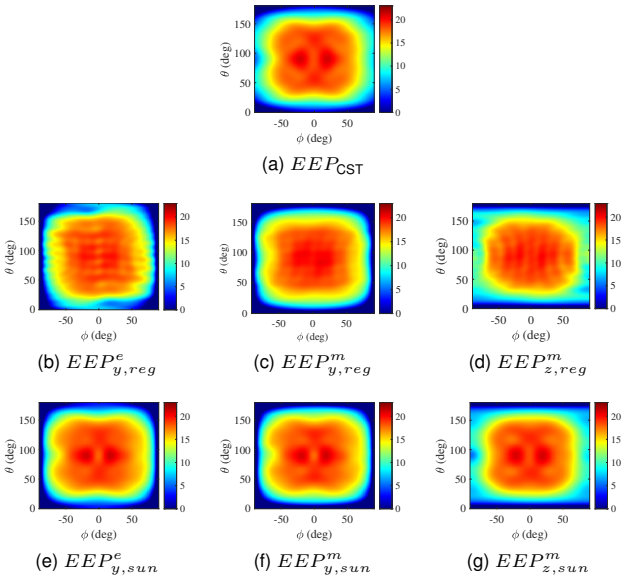

Fig. 5. EEP comparison (in terms of $|E|$) for the center element of the AUT where each topology comprises 81 IDs with $d_{ID} = 0.4\lambda$. The subscripts reg and sun stand for the regular and sunflower topology constrained IDM.

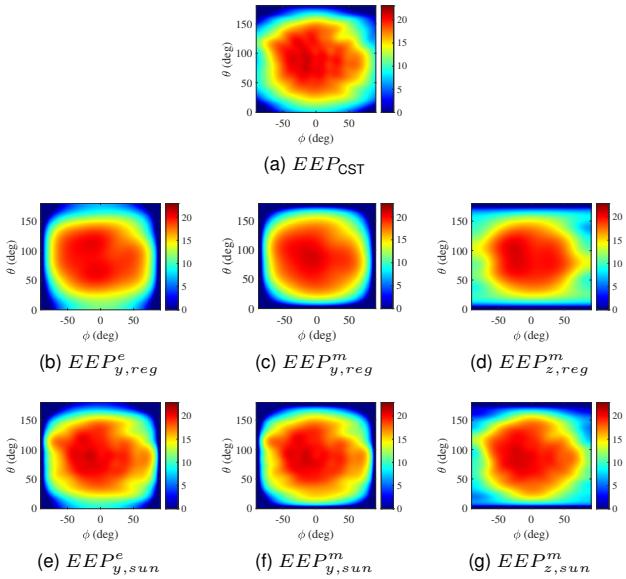

Fig. 6. EEP comparison (in terms of $|E|$) for the corner element of the AUT where each topology comprises 81 IDs with $d_{ID} = 0.4\lambda$. The subscripts reg and sun stand for the regular and sunflower topology constrained IDM.

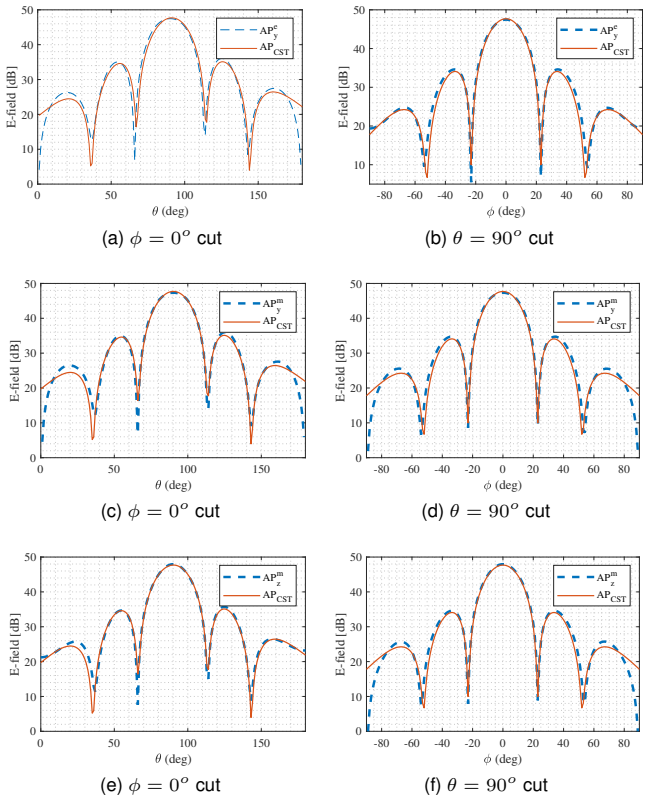

Fig. 7. Array far-field pattern (in terms of $|E|$) comparison for the constrained IDM with the proposed sunflower topology.

Nonetheless, the proposed topology achieves relatively good results, having an error of about -8 dB, while keeping the condition number below 140.

C. Array With Broadside Radiation

Further study was conducted for the reconstruction of the array pattern (AP) with the obtained EEPs by the proposed methodology. For this purpose, each EEP was predicted by using the sunflower topology with $p-$oriented $t-$dipoles in the constrained IDM. The obtained array pattern, AP^t_p, further is compared with the full-wave simulated array pattern, AP_{CST}.

Fig. 7 illustrates the $\theta = 90^o$ and $\phi = 0^o$ pattern cuts. While the prediction achieves good matching with the full-wave simulated pattern cuts, there are some disparities in the extreme angles. Since the prediction is based on absolute patterns, the phase information is missing during the reconstruction, causing potential errors in extreme angles.

IV. Conclusion

The sunflower array topology concept has been introduced in the constrained IDM problem to achieve computational efficiency with satisfying antenna far-field prediction accuracy. The impact of the type and orientation of dipoles on the MSE and the corresponding condition number were analyzed for a 5 by 5 patch array as the AUT. The use of magnetic dipoles oriented along the radiating edges of a patch is motivated. A case study with 81 IDs showed that the proposed topology decreases the MSE of the EEP prediction by 6.8 dB and 3.7 dB for the center and edge element, respectively. Moreover, the condition number is reduced by a factor of 10. Lastly, the broadside pattern of the AUT was reconstructed by the predicted EEPs with the proposed methodology and compared with the full-wave simulation result. A good agreement was observed on the pattern cuts; however, the prediction performance degraded at far side lobes. Future study will focus on the complex pattern predictions to overcome this degradation.

References

[1] S. M. Mikki and A. A. Kishk, "Theory and applications of infinitesimal dipole models for computational electromagnetics," *IEEE Transactions on Antennas and Propagation*, vol. 55, no. 5, pp. 1325–1337, 2007.

[2] W.-J. Zhao, B.-F. Wang, E.-X. Liu, H. B. Park, H. H. Park, E. Song, and E.-P. Li, "An effective and efficient approach for radiated emission prediction based on amplitude-only near-field measurements," *IEEE Transactions on Electromagnetic Compatibility*, vol. 54, no. 5, pp. 1186–1189, 2012.

[3] Y.-F. Shu, X.-C. Wei, J. Fan, R. Yang, and Y.-B. Yang, "An equivalent dipole model hybrid with artificial neural network for electromagnetic interference prediction," *IEEE Transactions on Microwave Theory and Techniques*, vol. 67, no. 5, pp. 1790–1797, 2019.

[4] M. Serhir, N. Ribière-Tharaud, and D. Picard, "Robust antenna diagnostics method using equivalent elemental dipoles and the spherical wave expansion," in *Proceedings of the Fourth European Conference on Antennas and Propagation*, 2010, pp. 1–5.

[5] S. Karimkashi, A. Kishk, and G. Zhang, "Modelling of aperiodic array antennas using infinitesimal dipoles," *IET Microwaves, Antennas & Propagation*, vol. 6, no. 7, pp. 761–767, 2012.

[6] J.-R. Regue, M. Ribó, J.-M. Garrell, and A. Martín, "A genetic algorithm based method for source identification and far-field radiated emissions prediction from near-field measurements for pcb characterization," *IEEE Transactions on Electromagnetic Compatibility*, vol. 43, no. 4, pp. 520–530, 2001.

[7] T. Sijher and A. Kishk, "Antenna modeling by infinitesimal dipoles using genetic algorithms," *Progress In Electromagnetics Research*, vol. 52, pp. 225–254, 2005.

[8] T. S. Sijher and A. A. Kishk, "Infinitesimal dipoles simulation of antennas using genetic algorithms," in *2004 10th International Symposium on Antenna Technology and Applied Electromagnetics and URSI Conference*, 2004, pp. 1–4.

[9] S. J. Yang, Y. D. Kim, D. W. Yi, N. H. Myung *et al.*, "Antenna modeling using sparse infinitesimal dipoles based on recursive convex optimization," *IEEE Antennas and Wireless Propagation Letters*, vol. 17, no. 4, pp. 662–665, 2018.

[10] M. Serhir, P. Besnier, and M. Drissi, "An accurate equivalent behavioral model of antenna radiation using a mode-matching technique based on spherical near field measurements," *IEEE Transactions on Antennas and Propagation*, vol. 56, no. 1, pp. 48–57, 2008.

[11] M. Serhir, P. Besnier, N. Ribière-Tharaud, and M. Drissi, "The use of infinitesimal dipoles and the spherical wave expansion for planar antennas modeling," in *Proceedings of the Fourth European Conference on Antennas and Propagation*, 2010, pp. 1–5.

[12] L. R. Turner, "Inverse of the vandermonde matrix with applications," Tech. Rep., No. NASA-TN-D-3547, 1966.

[13] W. Gautschi, "Optimally conditioned vandermonde matrices," *Numerische Mathematik*, vol. 24, pp. 1–12, 1975.

[14] M. C. Viganó, G. Toso, G. Caille, C. Mangenot, I. E. Lager *et al.*, "Sunflower array antenna with adjustable density taper," *International Journal of Antennas and Propagation*, vol. 2009, 2009.

[15] Y. Aslan, J. Puskely, J. H. J. Janssen, M. Geurts, A. Roederer, and A. Yarovoy, "Thermal-aware synthesis of 5G base station antenna arrays: an overview and a sparsity-based approach," *IEEE Access*, vol. 6, pp. 58 868–58 882, 2018.

[16] V. H. Vu and T. Tao, "The condition number of a randomly perturbed matrix," in *Proceedings of the 39th Annual ACM Symposium on Theory of Computing*, 2007, pp. 248–255.

[17] H. G. Moura, E. C. Junior, A. Lenzi, and V. C. Rispoli, "On a stochastic regularization technique for ill-conditioned linear systems," *Open Engineering*, vol. 9, no. 1, pp. 52–60, 2019.